Quasi-periodic solutions and homoclinic bifurcation in an impact inverted pendulum

Xiaoming Zhang[a] **Zhenbang Cao**[a] **Denghui Li**[b 1], **Celso Grebogi**[c] **Jianhua Xie**[a]

[a] ***School of Mechanics and Engineering, Southwest Jiaotong University, Chengdu, Sichuan, China, 610031***
[b] ***School of Mathematics and Statistics, Hexi University, Zhangye, Gansu, China, 734000***
[c] ***Institute for Complex Systems and Mathematical Biology King's College, University of Aberdeen, Aberdeen AB24 3UE, United Kingdom***

Abstract

We investigate a nonlinear inverted pendulum impacting between two rigid walls under external periodic excitation. Based on KAM theory, we prove that there are three regions (corresponding to different energies) occupied by quasi-periodic solutions in phase space when the periodic excitation is small. Moreover, the rotational quasi-periodic motion is maintained when the perturbation gets larger. The existence of subharmonic periodic solutions is obtained by the Aubry-Mather theory and the boundedness of all solutions is followed by the fact that there exist abundant invariant tori near infinity. To study the homoclinic bifurcation of this system, we present a numerical method to compute the discontinuous invariant manifolds accurately, which provides a useful tool for the study of invariant manifolds under the effect of impacts.

Keywords: KAM theory, quasi-periodic solution, impact system, computation of discontinuous invariant manifold

1. Introduction

The mathematical pendulum is one of the most studied classical nonlinear oscillators, which has very rich and intricate dynamics. Different dynamical systems' theories have been applied to the excited mathematical pendulum, such as KAM theory [15], Melnikov method [9, 10], variational method [19], and so on. See the comprehensive survey [19] and references therein for additional results on the forced pendulum.

In recent years, since non-smooth systems have attracted wide attention, the impact inverted pendulum has been studied by many authors. The impact inverted pendulum was simplified to a linear oscillator in [7] and the bifurcations of subharmonic periodic solutions were studied. The simplified system was also investigated in [25] by modifying the classical Melnikov method to show the existence of chaos. And the results in [25] were generalised by Du and Zhang [10] for more general nonlinear oscillators that have similar phase portraits as the impact inverted pendulum. See, e.g., [9, 11, 12, 26] for recent studies of piecewise smooth systems with homoclinic orbits.

[1]Corresponding author, Email address: lidenghui201111@126.com

Most of the known results are related to the applications of Melnikov method in impact systems and the bifurcations of periodic solutions. However, to the best of our knowledge, there is still no result on the existence of quasi-periodic solutions and the dynamics for the high energy case. This work aims to fill this gap. Since the dynamical system investigated in this work is non-smooth, the KAM theory cannot be applied directly. We thus introduce two settings to study this system. The exchange of the role of space and time allows us to smooth the dynamics of the system so that the KAM theory can be applied when some derivative estimates hold. More precisely, under suitable smoothness assumption for the perturbation, the dynamics of three regions of phase space, the first two corresponding to low energy and the last one corresponding to high energy, is reduced to twist maps. So the Moser's twist theorems imply the existence invariant curves, i.e., invariant tori in phase space. In addition, the existence of invariant curves near infinity implies that all solutions are bounded. Between two invariant curves, we use the method in [23, Section 5] to obtain a monotone twist map that preserves the boundaries. The existence of subharmonic periodic solutions is then obtained by the Aubry-Mather theory [3, 20].

The dynamics in the neighbourhood of unperturbed homoclinic orbit is very complicated. By the work in [10], the intersection of perturbed stable manifold and unstable manifold for such non-smooth system can be detected by the Melnikov method. We do not attempt to touch upon it in here. Instead, in this work, we modify the method for the computation of invariant manifolds for smooth systems [13, 17] to accommodate systems under the effect of impacts. Since the perturbed invariant manifolds are discontinuous, the traditional method is not applicable. Our modified parametric method provides an accurate and intuitive way to address homoclinic bifurcations in systems with impacts. As such, the tangency of unstable manifold and the impact surface can be detected directly since the unstable manifold is trapped in the neighbourhood of grazing point. In addition, we also discuss the symmetry of stable and unstable manifolds when a specific form of the system is given.

The remaining of this paper is organised as follows. In Section 2, we introduce the model and the main theoretical result of this paper. In Section 3, two settings of impact systems are presented to simplify the dynamics. The dynamics in the three regions are formally reduced to the near integrable ones in Section 4, and the necessary estimates, which are required by KAM theory, are presented in Appendix A. In Section 5, we verify the mathematical result by numerical simulation, and we also study the homoclinic bifurcation by the numerical method developed in Appendix B. The symmetry of perturbed stable and unstable manifolds is discussed when a specific form of the perturbation is assumed. Moreover, the tangency of the unstable manifold and the impact surface is identified since the unstable manifold is trapped in the neighbourhood of the grazing point when the perturbation is large. In Section 6, we present the conclusion and remarks.

2. The inverted pendulum with two rigid walls

We consider the following equation that describes the inverted pendulum presented in Figure 1:

$$\begin{aligned} \dot{x} =& y, \\ \dot{y} =& \frac{g}{l}\sin x - V_x(x,t), \end{aligned} \tag{2.1}$$

where $(x, y) \in [-\xi, \xi] \times \mathbb{R}$ and $0 < \xi < \pi/2$, g is the gravity constant, l is the length of the rod, $V : [-\xi, \xi] \times S^1$ ($S^1 = \mathbb{R}/\mathbb{Z}$) is a C^r ($r \geq 5$) function. We assume the impact

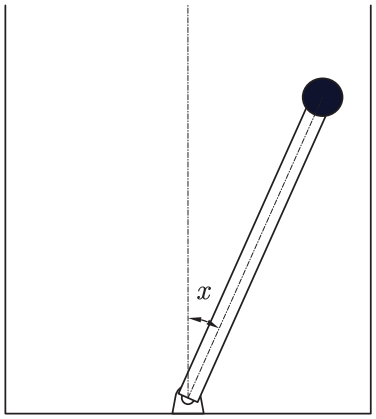

Figure 1: The mechanical model of the inverted pendulum between two rigid walls.

is elastic, i.e., $y \to -y$ when $|x| = \xi$. Without loss of generality, we take $g/l = 1$ in the remaining of the paper.

The Hamiltonian of system (2.1) is

$$H(y, x, t) = \frac{1}{2}y^2 + \cos x + V(x, t).$$

For the unperturbed system ($V(x,t) = 0$), the structure of the level set $\{(x, y) : \frac{1}{2}y^2 + \cos x = h\}$ is clear, see Figure 2. We define the following regions,

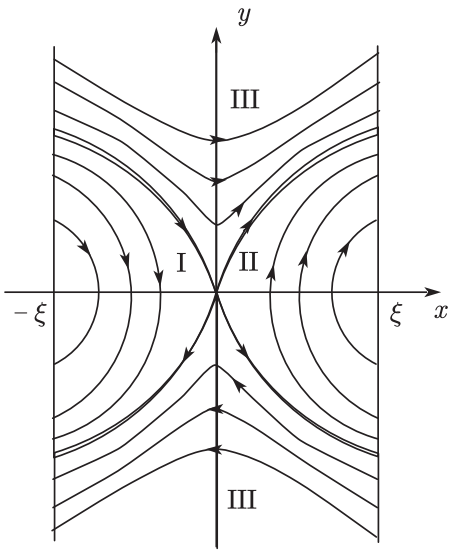

Figure 2: Phase portrait of (2.1) with V=0.

$$\left.\begin{array}{l} \text{I} := \{(x, y) : \cos\xi < h < 1 \text{ and } x < 0\}, \\ \text{II} := \{(x, y) : \cos\xi < h < 1 \text{ and } x > 0\}, \end{array}\right\} \to \text{ low energy}$$
$$\text{III} := \{(x, y) : h > 1\} \to \text{ high energy},$$

see Figure 2. Note that the dynamics of regions I and II are similar to a nonlinear oscillator with one-side impacts, and the region III is similar to the well-known Fermi-Ulam model [4, 5, 28].

Usually, one takes the impact surfaces as the sections to obtain the first return maps. The following theorem is the main theoretical result of this paper.

Theorem 2.1. (i) *There exists constant $\epsilon_0 > 0$ such that for any $\epsilon \in [0, \epsilon_0]$ the first return map of the surface*

$$\{(x, y, t) : x = -\xi, y \in [\sqrt{2h_0 - 2\cos\xi} + O(\epsilon), \sqrt{2h_1 - 2\cos\xi} + O(\epsilon)]\}$$

has invariant curves with positive measure if

$$|\frac{\partial^{k+l}}{\partial x^k \partial t^l} V| \leq \epsilon \leq \epsilon_0 \tag{2.2}$$

on $[-\xi, \xi] \times S^1$ for all $0 \leq k + l \leq 5$, where $[h_0, h_1] \subset (\cos\xi, 1)$ is a nonempty interval, k, l are nonnegative integers. Moreover, the constant ϵ_0 does only depend on ξ, h_0, h_1, and the measure of invariant curves tends to the measure of the set

$$S^1 \times [\sqrt{2h_0 - 2\cos\xi} + O(\epsilon), \sqrt{2h_1 - 2\cos\xi} + O(\epsilon)]$$

as ϵ tends to zero. The results also hold (even the constant ϵ_0 will not change) for the surface

$$\{(x, y, t) : x = \xi, y \in [\sqrt{2h_0 - 2\cos\xi} + O(\epsilon), \sqrt{2h_1 - 2\cos\xi} + O(\epsilon)]\}.$$

(ii) *There exists constant $\epsilon_1 > 0$ such that the first return map of the surface*

$$\{(x, y, t) : x = \xi, y \in [-\frac{4\xi}{\epsilon} + O(\epsilon), -\frac{2\xi}{\epsilon} + O(\epsilon)]\}$$

has invariant curves for any $\epsilon \in (0, \epsilon_1)$. In particular, all solutions are bounded for all time, i.e.,

$$\sup_{t\in\mathbb{R}}(|x(t)| + |y(t)|) < \infty.$$

3. The equivalent form of impact systems and a non-smooth action-angle coordinate

Before getting into the technical details, we first introduce two settings to simplify the impact systems as done in this work. The first setting allows us to treat the impact systems as having a non-smooth Hamiltonian function [28, 29], and the second setting is to carry out a non-smooth action-angle coordinate change that reduces the dynamics to a near integrable one.

3.1. The equivalent form of impact systems

Consider the following system

$$\begin{cases} \dot{x} = y, \\ \dot{y} = -w_x(x, t), \end{cases} \tag{3.1}$$

where $(x, y) \in [0, \infty) \times \mathbb{R}$, $w : \mathbb{R}^2 \to \mathbb{R}$ is a C^2 function. Suppose that there exists a rigid wall at $x = 0$ and the impact is elastic, i.e., $y \to -y$ when $x = 0$. The equivalent form of such system is described by the following equations:

$$\begin{cases} \dot{x} = y, \\ \dot{y} = -w_x(x,t), \end{cases} \quad x > 0, \ (*) \qquad \begin{cases} \dot{x} = y, \\ \dot{y} = w_x(-x,t), \end{cases} \quad x < 0 \ (**) \tag{3.2}$$

In fact, if

$$(x(t, t_0, x_0, y_0), y(t, t_0, x_0, y_0))$$

is the solution of $(*)$ when the initial conditions are $x(t_0) = x_0 \geq 0, \ y(t_0) = y_0$, where $t \in [t_0, t_1]$ and $x(t, t_0, x_0, y_0) \geq 0$ for $t \in [t_0, t_1]$, then

$$(-x(t, t_0, x_0, y_0), -y(t, t_0, x_0, y_0))$$

is the solution of $(**)$ with initial conditions $x(t_0) = -x_0 \leq 0, y(t_0) = -y_0$. Let a solution of (3.1) be

$$\{(x^{(1)}(t), y^{(1)}(t)), (x^{(2)}(t), y^{(2)}(t)), ..., (x^{(n)}(t), y^{(n)}(t)), ...\},$$

where for any i, $t \in [t_i, t_{i+1}]$, $(x^{(i)}(t), y^{(i)}(t))$ is the solution of (3.1), and the following conditions hold

$$x^{(i)}(t_i) = x^{(i)}(t_{i+1}) = 0, \ y^{(i)}(t_{i+1}) = -y^{(i+1)}(t_{i+1}), x^{(i)}(t) > 0 \text{ when } t \in (t_i, t_{i+1}).$$

By the analysis above,

$$\{(x^{(1)}(t), y^{(1)}(t)), (-x^{(2)}(t), -y^{(2)}(t)), (x^{(3)}(t), y^{(3)}(t)), (-x^{(4)}(t), -y^{(4)}(t)), ...\},$$

is a solution of (3.2). See Figure 3 for an intuitive illustration.

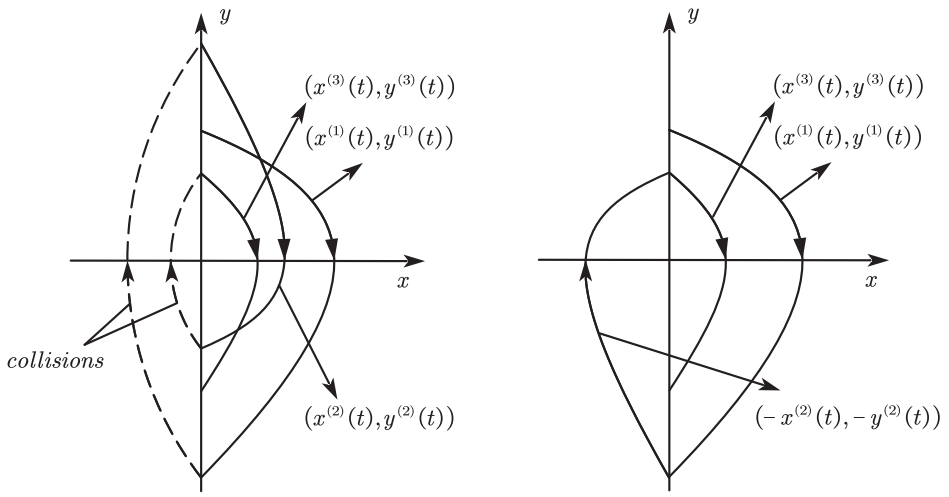

(a) An orbit of (3.1) (b) The corresponding orbit of (3.2)

Figure 3: The equivalence of (3.1) and (3.2)

Finally, note that the equivalent system (3.2) is corresponding to a Hamiltonian system with the non-smooth Hamiltonian

$$K(y, x, t) = \frac{1}{2}y^2 + w(|x|, t).$$

Remark 1. *If the system* (3.1) *has two rigid walls, for example* $x = 0$ *and* $x = 2\xi$*, the trajectories of the system with Hamiltonian* $K(y, x, t)$ *from* $x = -2\xi$ *to* $x = 2\xi$ *correspond to the trajectories of the impact system from* $x = 2\xi$ *to* $x = 0$ *and then from* $x = 0$ *to* $x = 2\xi$*, see Figure 4. Therefore, if we take the section* $\{(x, y, t) : x = 2\xi, y < 0\}$ *to study the system* (3.1)*, then we can establish the Poincaré map equivalently by taking the map of Hamiltonian system* $K(y, x, t)$ *from* $\{(x, y, t) : x = -2\xi, y > 0\}$ *to* $\{(x, y, t) : x = 2\xi, y > 0\}$*. We will use this fact in studying the region III, where the trajectories will collide with both* $x = -\xi$ *and* $x = \xi$ *when the initial energy is large.*

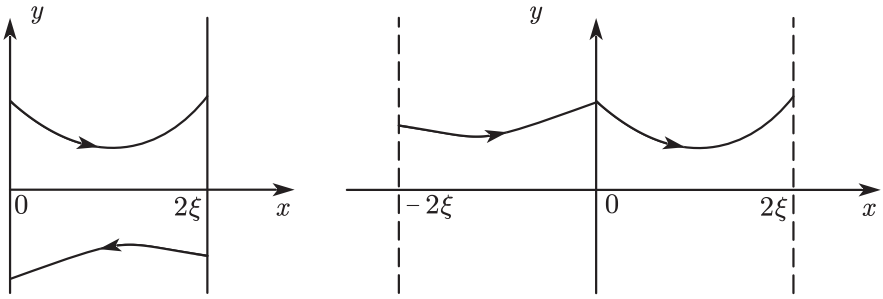

Figure 4: Level set of H.

3.2. A non-smooth action-angle coordinate

We consider the non-smooth action-angle coordinate (see [2]) in region I. The case of region II can be obtained by reflecting the orbit about $x = 0$. After moving the wall from $x = -\xi$ to $x = 0$, we study the equivalent unperturbed system with Hamiltonian

$$H(y, x) = \frac{1}{2}y^2 + \cos(|x| - \xi).$$

The structure of the level set $\{(x, y) : \frac{1}{2}y^2 + \cos(|x| - \xi) = h \text{ and } |x| < \xi\}$ for $h \in (\cos\xi, 1)$ is presented in Figure 5. In this Subsection, we assume $h \in (\cos\xi, 1)$ and $|x| < \xi$.

Let

$$I(h) = 4\sqrt{2}\int_0^{\arccos h+\xi} \sqrt{h - \cos(x - \xi)}dx.$$

Observe that $I(h)$ is the area of the domain surrounded by the level set $\{(x, y) : \frac{1}{2}y^2 + \cos(|x| - \xi) = h \text{ and } |x| < \xi\}$. It turns out that $I(h)$ is smooth and $I'(h) > 0$ for $h \in (\cos\xi, 1)$, see Lemma A.1. Hence, we can reverse it and denote the inverse by $h(I)$. Let

$$D = \{(x, y) : \frac{1}{2}y^2 + \cos(|x| - \xi) = h,\ |x| < \xi,\ \cos\xi < h < 1\}. \tag{3.3}$$

We shall now define a symplectic transformation $\Phi : (I, \theta) \mapsto (x, y)$, where $I \in (0, I(1)), \theta \in S^1, (x, y) \in D$.

In the domain of $x \geq 0$, let the generating function be defined by

$$S(y, I) = \int_y^{\sqrt{2(h(I)-\cos\xi)}} x(I, s)ds,$$

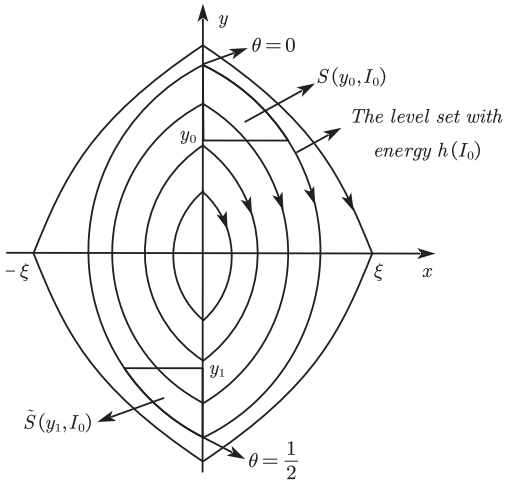

Figure 5: Level set of H and the definitions of generating functions S and $\tilde{S}$

where $y \in [-\sqrt{2(h(I)-\cos\xi)}, \sqrt{2(h(I)-\cos\xi)}]$ and $x(I,y)$ satisfies $h(I) = \frac{1}{2}y^2 + \cos(x(I,y) - \xi)$, i.e.,

$$x(I,y) = -\arccos(h(I) - \frac{1}{2}y^2) + \xi.$$

The area of the shadowed region in the upper right of Figure 5 is the value of $S(y_0, I_0)$.

The map Φ in this domain is defined by

$$x = -S_y(y,I),\ \theta = S_I(y,I). \tag{3.4}$$

Since

$$\frac{\partial^2 S}{\partial I \partial y} = -\frac{h'(I)}{\sqrt{1-(h(I)-\frac{1}{2}y^2)}} < 0 \tag{3.5}$$

for $y \in [-\sqrt{2(h(I)-\cos\xi)}, \sqrt{2(h(I)-\cos\xi)}]$, we can determine $y(I,\theta)$ from second formula of (3.4) and then $x(I,\theta)$ is defined by the first formula of (3.4). It turns out that both $x(I,\theta)$ and $y(I,\theta)$ are C^∞ functions since $S(y,I)$ is a C^∞ function for $x \geq 0$. Note that $\theta \in [0,1/2]$ when $x \geq 0$. In fact, by definitions of S and θ, we have

$$\theta(\sqrt{2(h(I)-\cos\xi)}, I) = \frac{\partial}{\partial I} S(\sqrt{2(h(I)-\cos\xi)}, I) = 0,$$
$$\theta(-\sqrt{2(h(I)-\cos\xi)}, I) = \frac{\partial}{\partial I} S(-\sqrt{2(h(I)-\cos\xi)}, I) = \frac{\partial}{\partial I}(\frac{1}{2}I) = \frac{1}{2}.$$

Since $y \in [-\sqrt{2(h(I)-\cos\xi)}, \sqrt{2(h(I)-\cos\xi)}]$, then $\theta \in [0,1/2]$ is followed by the fact $\partial\theta/\partial y = \partial^2 S/\partial I \partial y < 0$.

Similarly, in the domain of $x \leq 0$, let

$$\tilde{S}(y,I) = \frac{1}{2}I + \int_y^{-\sqrt{2(h-\cos\xi)}} \tilde{x}(s,I)ds,$$

where $y \in [-\sqrt{2(h(I)-\cos\xi)}, \sqrt{2(h(I)-\cos\xi)}]$,

$$\tilde{x}(I,y) = \arccos(h(I) - \frac{1}{2}y^2) - \xi.$$

The map Φ in this domain is defined by

$$x = -\tilde{S}_y(y, I),\ \theta = \tilde{S}_I(y, I). \tag{3.6}$$

Since

$$\frac{\partial \tilde{S}^2}{\partial I \partial y} = \frac{h'(I)}{\sqrt{1 - (h(I) - \frac{1}{2}y^2)}} > 0 \tag{3.7}$$

for $y \in [-\sqrt{2(h(I) - \cos\xi)}, \sqrt{2(h(I) - \cos\xi)}]$, we can determine $y(I, \theta)$ from the second formula of (3.6) and then $x(I, \theta)$ is defined by the first formula of (3.6). Therefore, the map Φ is well defined. We can similarly show that $\theta \in [1/2, 1]$ when $x \leq 0$.

If (x, y) rotates along the level curve clockwise and return to itself, then the generation function increases by I and θ increases by 1. Hence $\theta \in S^1$. To see the non-smoothness of Φ in $\theta \in \{0, \frac{1}{2}\}$, for example, by (3.4) and (3.6) we have

$$\frac{\partial y}{\partial \theta} = \frac{1}{S_{Iy}} \text{ for } x \geq 0,\ \frac{\partial y}{\partial \theta} = \frac{1}{\tilde{S}_{Iy}} \text{ for } x \leq 0. \tag{3.8}$$

Note that when $x \to 0^+$ and $y \to \sqrt{2(h - \cos\xi)}$, we have $\theta \to 0^+$; when $x \to 0^-$ and $y \to \sqrt{2(h - \cos\xi)}$, we have $\theta \to 1^-$, i.e., $\theta \to 0^-$. The formulas (3.5) and (3.7) yield

$$\lim_{\theta \to 0^+} \frac{\partial y}{\partial \theta}(I, \theta) = -\frac{\sqrt{1 - \cos\xi}}{h'(I)} \neq \lim_{\theta \to 0^-} \frac{\partial y}{\partial \theta}(I, \theta) = \frac{\sqrt{1 - \cos\xi}}{h'(I)}.$$

Therefore, the transformation Φ is non-smooth at $\theta = 0$. The case of $\theta = \frac{1}{2}$ is similar.

For convenience, we summarise the above discussion as following:

Proposition 3.1. *The non-smooth coordinate change $\Phi : (I, \theta) \to (x, y)$ is a C^∞ map for $I \in (0, I(1))$ and $\theta \in [0, \frac{1}{2}]$ or $\theta \in [\frac{1}{2}, 1]$. In particular, $x(I, \theta)$ is C^r $(r \geq 1)$bounded for $(I, \theta) \in [I(h_0), I(h_1)]$ and $\theta \in [0, \frac{1}{2}]$, where $[h_0, h_1] \subset (\cos\xi, 1)$.*

4. The establishment of twist maps in the regions I,III and applications of twist map theorems

In this Section, we choose suitable sections so that the Poincaré maps of these sections in regions I and III are near integrable twist maps. Moser's twist theorems imply the existence invariant tori in the phase space. The produces in here are formal, and the necessary estimates are presented in Appendix A.

4.1. The quasi-periodic motions in regions I and II

We first consider the one-side impact motion when V is small. Since the cases in the regions I and II are similar, we only study the former one.

Usually, we can take the Poincaré map with the impact section $\{(x, y, t) : x = -\xi, y > 0\}$ to study the dynamics in the region I. Ignoring the constant coordinate $x = -\xi$, the Poincaré map can be decomposed into:

$$(y_0, t_0) \xrightarrow{\text{(i)}} (-y_1, t_1) \xrightarrow{\text{(ii)}} (y_1, t_1), \tag{4.1}$$

where $y_0, y_1 > 0$, the map (i) is the action of the flow of (2.1), the map (ii) is the impact map. The key to establish the twist map is the estimate of $t_1 - t_0$. If we use the action-angle coordinate in region I, θ increases from 0 to 1/2 when (y_0, t_0) arrives at $(-y_1, t_1)$.

Hence, if we can choose θ as the new time, then the time that the map (i) spends will be a constant. Choosing energy and time as variants, the Poincaré map (4.1) becomes

$$(H_0, t_0) \xrightarrow{\text{(i)}} (H_1, t_1) \xrightarrow{\text{(ii)}} (H_1, t_1),$$

where $H_i = H(y_i, -\xi, t_i)$, the map (ii) becomes into identity map since the impact does not change the energy. In the following, when V is small, we will obtain a Hamiltonian system such that (H, t, θ) is the momentum, position, and time respectively. Therefore, the Poincaré map (4.1) is a time-$\frac{1}{2}$-map.

Recall that the Hamiltonian of the inverted pendulum is

$$H(y, x, t) = \frac{1}{2}y^2 + \cos x + V(x, t).$$

Moving the wall $x = -\xi$ to $x = 0$, we study the equivalent system with Hamiltonian

$$H(y, x, t) = \frac{1}{2}y^2 + \cos(|x| - \xi) + V(|x| - \xi, t), \tag{4.2}$$

see Section 3.1 for the equivalence. Using the non-smooth action-angle coordinate (I, θ) in Section 3.2, the Hamiltonian H in region I is

$$H(I, \theta, t) = h(I) + V(|x(I, \theta)| - \xi, t). \tag{4.3}$$

Since we only consider the case of $\theta \in [0, 1/2]$, i.e., $x \geq 0$, we can remove the absolute value in (4.3). Following Arnold [1], Levi [16], and Zharnitsky [28, 29], we exchange the roles of position and time (resp. Hamiltonian and momentum). More specifically, since the integral curves of the Hamiltonian systems are invariantly associated with the differential form

$$Id\theta - Hdt = -(Hdt - Id\theta),$$

we can choose (I, H, t, θ) as a new Hamiltonian, momentum, position, and time, respectively. Since V is small and $h'(I) > 0$, we can get the formal formula of I by (4.3) and the Implicit Function Theorem

$$I(H, t, \theta) = I(H) + I_1(H, t, \theta),$$

where $I(\cdot)$ is the inverse of $h(\cdot)$, see Section 3.2. The corresponding equations are

$$\begin{aligned} \frac{dt}{d\theta} &= I'(H) + \frac{\partial I_1}{\partial H}(H, t, \theta), \\ \frac{dH}{d\theta} &= -\frac{\partial I_1}{\partial t}(H, t, \theta). \end{aligned} \tag{4.4}$$

Integrating (4.4) from $\theta = 0$ to $\theta = \frac{1}{2}$, we obtain the Poincaré map

$$\begin{aligned} t_1 &= t_0 + \frac{1}{2}I'(H_0) + N_1(t_0, H_0), \\ H_1 &= H_0 + N_2(t_0, H_0). \end{aligned} \tag{4.5}$$

We claim that there exist positive constants ϵ_0 and a such that for any $\epsilon \in [0, \epsilon_0]$ the following estimates

$$I''(H) \geq a > 0 \text{ and } |\frac{\partial^{k+l}}{\partial H^k \partial t^l} N_i(H, t)| \leq C\epsilon \tag{4.6}$$

hold on $(H,t)\in[h_0,h_1]\times S^1$ for all $0\le k+l\le 4$, $i=1,2$, if

$$|\frac{\partial^{k+l}}{\partial x^k\partial t^l}V|\le\epsilon\le\epsilon_0$$

holds on $(x,t)\in[-\xi,\xi]\times S^1$ for all $0\le k+l\le 5$, where C is a constant independent of ϵ, $[h_0,h_1]\subset(\cos\xi,1)$ is a nonempty interval and a only depends on h_0 and h_1.

Note that the intersection property, in which a homotopic nontrivial circle in $[h_0,h_1]\times S^1$ has nonempty intersection with its image, holds since we choose the time section of a Hamiltonian flow, see [28, Section 8] or [8, Lemma 4]. Hence, the map (4.5) satisfies the conditions of Moser's twist theorem [21] (see [24] for the C^4 version), which implies that there exist lots of invariant curves.

To show Theorem 2.1 **(i)** holds, we still have to back to the Poincaré map of the section $\{(x,y,t):x=-\xi,y>0\}$ (we have moved $x=0$ back to $x=-\xi$). By (4.2) and (4.5), the Poincaré map is

$$(t,\frac{1}{2}y^2+\cos\xi+O(\epsilon))\to(t+\frac{1}{2}I'(h(y,-\xi)+O(\epsilon))+O(\epsilon),\frac{1}{2}y^2+\cos\xi+O(\epsilon)),$$

where $y^2/2+\cos\xi+O(\epsilon)\in[h_0,h_1]$, $h(y,x)=y^2/2+\cos(x)$. Since $y>0$, the above map in coordinate (t,y) is

$$\begin{aligned}t_1&=t_0+\frac{1}{2}I'(h(y_0,-\xi))+O(\epsilon),\\ y_1&=y_0+O(\epsilon),\end{aligned}$$

where $(t_0,y_0)\in S^1\times[\sqrt{2h_0-2\cos\xi}+O(\epsilon),\sqrt{2h_1-2\cos\xi}+O(\epsilon)]$. Then Moser's twist theorem [24] yields Theorem 2.1 **(i)**.

4.2. The quasi-periodic motions on regions III: the large energy case

We consider the motions that have impacts both with $x=-\xi$ and $x=\xi$, i.e., the initial energy is large. The case in here is similar in Section 3.1. After moving the wall from $x=-\xi$ to $x=0$, the positions of the walls are $x=0$ and $x=2\xi$. By Section 3.1 and Remark 1, We consider the Hamiltonian system

$$H(y,x,t)=\frac{1}{2}y^2+\cos(|x|-\xi)+V(|x|-\xi,t)$$

on $\mathbb{R}\times[-2\xi,2\xi]\times S^1$. In the high energy region, we can use position x as time and the map from $\{(x,y,t):x=-2\xi,y>0\}$ to $\{(x,y,t):x=2\xi,y>0\}$ can be obtained by integrating a near integrable Hamiltonian system formally. By Remark 1, this map is the Poicaré map of system (2.1) with the section $\{(x,y,t):x=2\xi,y<0\}$.

By the invariance of integral curves of Hamiltonian systems with the differential form

$$\epsilon(ydx-Hdt)=\epsilon ydx-\epsilon^2Hd\frac{t}{\epsilon},$$

we can choose $(\epsilon^2H,\epsilon y,x,\frac{t}{\epsilon})=(F,p,q,T)$ as a new Hamiltonian, momentum, position, and time, respectively. See [28, 29] for similar coordinate transformations for billiard system and Fermi-Ulam model. Note that, e.g., $p\in[1,2]$ is corresponding to $y\in[\frac{1}{\epsilon},\frac{2}{\epsilon}]$, i.e., the energy is large. We have

$$F(p,q,T)=\frac{1}{2}p^2+\epsilon^2(\cos(|q|-\xi)+V(|q|-\xi,\epsilon T)).\tag{4.7}$$

We can still choose the position as the new time to eliminate the implicit arrival time at the impact surfaces. More specifically, since

$$\epsilon(pdq - FdT) = -(Fd\epsilon T - \epsilon pdq),$$

we can choose $(\epsilon p, F, \epsilon T, q) = (M, P, Q, s)$ as a new Hamiltonian, momentum, position, and time, respectively. By (4.7), we have

$$p = \sqrt{2F} + \epsilon^2 G(F, |q|, \epsilon T).$$

Hence, we have

$$M(P, Q, s) = \epsilon\sqrt{2P} + \epsilon^3 G(P, Q, |s|).$$

The corresponding Hamiltonian equation is

$$\begin{aligned} \frac{dQ}{ds} &= \frac{\epsilon}{\sqrt{2P}} + \epsilon^3 \frac{\partial G}{\partial P}, \\ \frac{dP}{ds} &= -\epsilon^3 \frac{\partial G}{\partial Q}. \end{aligned} \tag{4.8}$$

Let $\frac{4\xi}{\sqrt{2P}} = \bar{P}$. Then equation (4.8) in coordinate $(\bar{P}, Q)$ becomes

$$\begin{aligned} \frac{dQ}{ds} &= \frac{\epsilon \bar{P}}{4\xi} + \epsilon^3 G_1(\bar{P}, Q, |s|), \\ \frac{d\bar{P}}{ds} &= \epsilon^3 G_2(\bar{P}, Q, |s|), \end{aligned} \tag{4.9}$$

where

$$G_1(\bar{P}, Q, |s|) = \frac{\partial G}{\partial P}(\frac{8\xi^2}{\bar{P}^2}, Q, |s|), G_2(\bar{P}, Q, |s|) = \frac{\bar{P}^3}{16\xi^2}\frac{\partial G}{\partial Q}(\frac{8\xi^2}{\bar{P}^2}, Q, |s|).$$

Integrating (4.9) from $s = -2\xi$ to $s = 2\xi$, we obtain the Poincaré map

$$\begin{aligned} Q_1 &= Q_0 + \epsilon \bar{P} + \epsilon^3 R_1(Q_0, \bar{P}_0, \epsilon), \\ \bar{P}_1 &= \bar{P}_0 + \epsilon^3 R_2(Q_0, \bar{P}_0, \epsilon). \end{aligned} \tag{4.10}$$

We assert that there exists constant $\epsilon_1 > 0$ such that for any $\epsilon \in (0, \epsilon_1)$ the following estimate

$$\epsilon^3 |\frac{\partial^{k+l}}{\partial Q^k \partial \bar{P}^l} R_i(Q, \bar{P}, \epsilon)| \leq \epsilon^{1+\nu} \tag{4.11}$$

holds on $(\bar{P}, Q) \in [1, 2] \times S^1$ for all $0 \leq k + l \leq 4$, $i = 1, 2$, where $\nu > 0$ is a constant independent of ϵ.

Hence, the map (4.10) satisfies the conditions of Moser's small twist theorem [24]. Again, the intersection property holds for the time section map for (4.8), then it holds for (4.10) since these maps are conjugate.

By retracing the transformations, the return map of the surface $\{(x, y, t) : x = \xi, y < 0\}$, which has the following form

$$\begin{aligned} t_1 &= t_0 - \frac{4\xi}{y_0} + O(\epsilon^2), \\ y_1 &= y_0 + O(\epsilon^2) \end{aligned}$$

for $(y_0, t_0) \in [-\frac{4\xi}{\epsilon} + O(\epsilon), -\frac{2\xi}{\epsilon} + O(\epsilon)] \times S^1$, possesses lots of invariant curves when $\epsilon \in (0, \epsilon_1)$, which yields Theorem 2.1 **(ii)**.

Remark 2. *Using energy (see* (4.2)*) and time as variants, we have shown that the Poincaré map with section* $\{(x, y, t) : x = \xi, y < 0\}$ *has abundant invariant curves in*

$$\mathcal{U}_\epsilon := [\frac{4\xi^2}{\epsilon^2} + O(1), \frac{16\xi^2}{\epsilon^2} + O(1)] \times S^1.$$

Take a sequence $\{\epsilon_i\}_{i\in\mathbb{N}}$ *such that* $\epsilon_i \to 0$ *as* $i \to \infty$ *and* $\mathcal{U}_{\epsilon_i} \cap \mathcal{U}_{\epsilon_j} = \emptyset$ *for* $i \neq j$*. Since* $\mathcal{U}_{\epsilon_i}$ *can near* $\infty \times S^1$ *arbitrarily as* $i \to \infty$*, there exist invariant curves in the region with arbitrary high energy, which provide barriers for any solution of system* (2.1)*.*

Remark 3. *Both the map* (4.5) *and the map obtained by integrating equation* (4.8) *satisfy the monotone twist condition, then we can use the method in [23, Section 5] between two invariant curves to obtain a standard monotone twist map which preserves the boundaries. Therefore, the existence of Aubry-Mather sets, including Birkhoff* (p, q) *periodic orbits, generalised quasi-periodic solution for any irrational number contained in rotational interval, and homoclinic,heteroclinic connections between periodic orbits is directly followed by the Aubry-Mather theory [3, 20].*

Conclusively, the Theorem 2.1 is followed by the Moser's twist theorem and small twist theorem as long as the estimates (4.6) and (4.11) hold. The proof of (4.6) and (4.11) is contained in Appendix A.

5. The global dynamics of the inverted pendulum via numerical methods

In this Section, we give numerical evidence of Theorem 2.1, and we also show the perturbed unstable and stable manifolds via the revised parametric method in Appendix B. In such a manner, the global dynamics of the inverted pendulum can be understood in an intuitive way.

Without loss of generality, we assume $V(x, t)$ is π-periodic and let $V(x, t) = \epsilon x \cos(2t)$ in this Section, where ϵ is a constant. Fixed $\xi = \pi/4$. When ϵ is small, there exists lots of quasi-periodic solutions in regions I, II and III by Theorem 2.1. Let $\epsilon = 0.1$. Figure 6, Figure 7, and Figure 8 show the Poincaré maps that have $\{(x, y, t) : x = -\xi, y > 0\}$, $\{(x, y, t) : x = \xi, y < 0\}$, and the time $t = 0 \pmod{\pi}$ as Poincaré sections, respectively, where different colours denote different initial conditions in these figures. It can be seen that the numerical simulations are validated by Theorem 2.1.

When ϵ gets large, the invariant tori in regions I and II break up. However, in the region for $|y|$ large enough, the dynamics is still near integrable. For example, let $\epsilon = 0.8$, Figure 9 shows the Poincaré map that has $\{(x, y, t) : x = -\xi, y > 0\}$ as a section. It can be seen that there is chaotic behaviour when y is small while the invariant curves are abundant for the larger energy.

To study the dynamics in the neighbourhood of unperturbed homoclinic orbit, we use the method in Appendix B to compute the perturbed invariant manifold.

Let $\epsilon = 0.1$. Let ϕ be the time-π-map from $t = 0$ to $t = \pi$. First we use the shooting method to obtain the fixed point of ϕ perturbed from $(0, 0)$:

$$(x^*, y^*) = (0.02000020577986, 0).$$

The saddle type π-periodic solution is shown in Figure 10. The eigenvalues and the corresponding eigenvectors of the matrix $\mathrm{D}\phi((x^*, y^*))$ are:

$$\lambda_1 = 23.1370608417321,\ v_1 = (0.707127994451262, 0.7070855672854144),$$

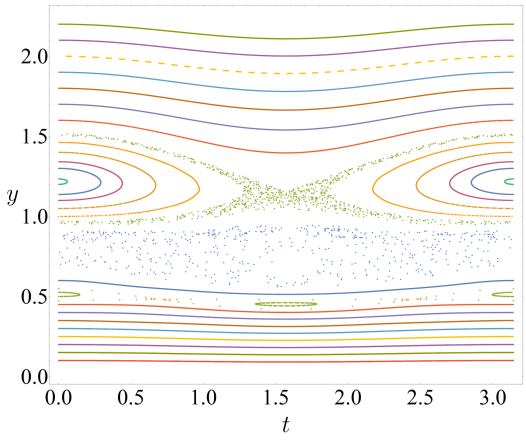

Figure 6: Poincaré maps with section $\{(x, y, t) : x = -\xi, y > 0\}$ when $\epsilon = 0.1$.

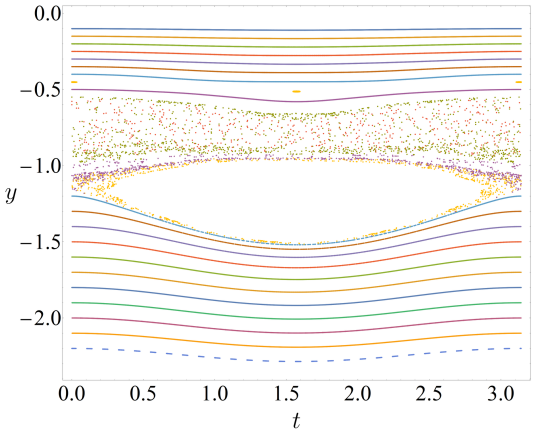

Figure 7: Poincaré maps with section $\{(x, y, t) : x = \xi, y < 0\}$ when $\epsilon = 0.1$.

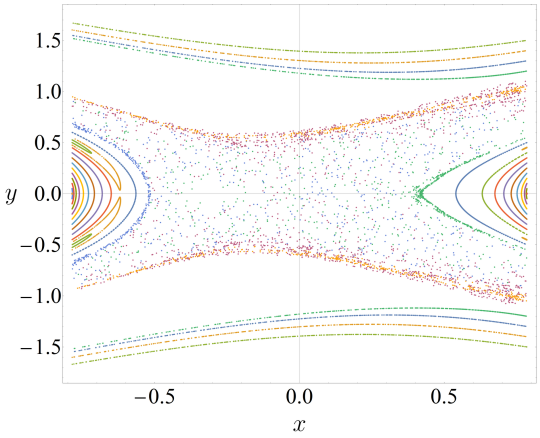

Figure 8: Poincaré maps with section $t = 0 \pmod{\pi}$ when $\epsilon = 0.1$.

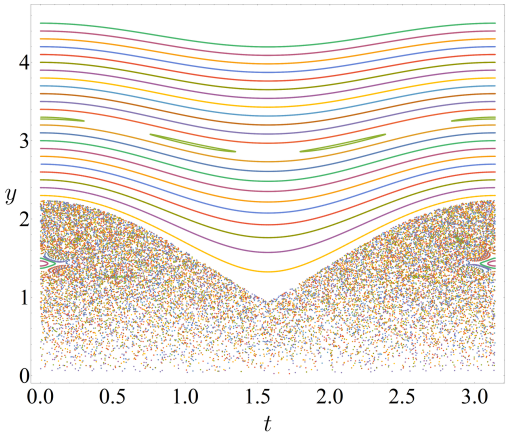

Figure 9: Poincaré maps with section $\{(x, y, t) : x = -\xi, y > 0\}$ when $\epsilon = 0.8$.

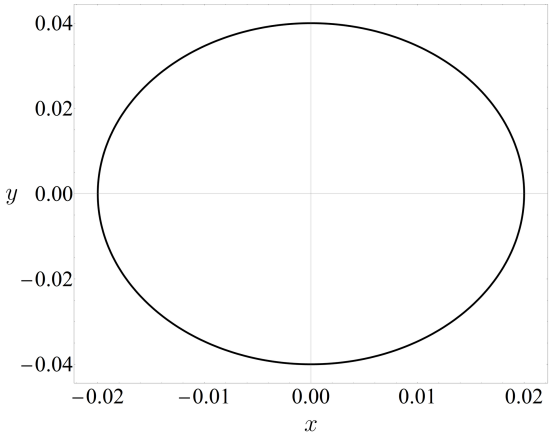

Figure 10: The saddle type periodic solution perturbed from $(0, 0)$.

$$\lambda_2 = 0.043220709991704,\ v_2 = (-0.707127991753206, 0.707085569983632).$$

We apply the procedures **(1)-(5)** specified in the Appendix B iteratively, for ϕ and for a line segment that has 0.01 length and the same direction as v_1. We choose 100 points uniformly in this segment. Let $\delta_1 = 10^{-6}$, $\delta_2 = 0.005$, and $m = 10$ (see **(2)-(4)** in Appendix B). After 4-times iterations, we show the parametric curves, i.e., a branch of the unstable manifold, for all steps in Figure 11. Some magnifications of Figure 11 are shown in Figure 12. The intersections of the unstable manifold with the impact surfaces are well localised, see (a) in Figure 12.

Similarly, we can compute another branch of the unstable manifold and the stable manifold. Figure 13 shows the complicated intersections of stable and unstable manifolds, and magnifications of Figure 13 are shown in Figure 14.

When the perturbation is small, the stable and unstable manifolds are symmetric about $y = 0$. In fact, one can verify that

$$(\varphi_1(0, -t, x_0, -y_0), -\varphi_2(0, -t, x_0, -y_0)) = (\varphi_1(0, t, x_0, y_0), \varphi_2(0, t, x_0, y_0))$$

since $V(x, t) = \epsilon \cos(2t)$, where $(\varphi_1(0, t, x_0, y_0), \varphi_2(0, t, x_0, y_0))$ is the solution of (2.1) with initial conditions $x(0) = x_0,\ y_0 = y_0$. Since the impacts are elastic, the symmetry is not destroyed. In particular, we have

$$(\phi_1(x, y), -\phi_2(x, y)) = \phi^{-1}(x, -y),$$

where ϕ_i is a component of ϕ. Let $\mathcal{R}(x, y) = (x, -y)$. Then the above identify can be represented by

$$\mathcal{R} \circ \phi = \phi^{-1} \circ \mathcal{R}.$$

It follows that if A is a invariant set of ϕ, then $\mathcal{R}(A)$ is also ϕ-invariant. In particular, we have

$$\phi^{-1}(x^*, -y^*) = (x^*, -y^*).$$

Since the fixed point (x^*, y^*) is unique in the neighbourhood of $(0, 0)$ when the perturbation is small, we must have $y^* = 0$. If (x, y) lies on the stable manifold, i.e.,

$$\phi^n(x, y) \to (x^*, 0) \text{ as } n \to \infty,$$

then

$$(\phi_1^n(x, y), -\phi_2^n(x, y)) \to (x^*, 0) \text{ as } n \to \infty,$$

where ϕ_i^n is a component of ϕ^n. Therefore,

$$\phi^{-n}(x, -y) \to (x^*, 0) \text{ as } n \to \infty,$$

i.e., $(x, -y)$ lies on the unstable manifold. Hence, the stable manifold and unstable manifold are symmetric about $y = 0$. Figure 13, Figures 14 (b) and (d) verify this fact.

Conclusively, when the perturbation is small, the dynamics of the impact inverted pendulum can be divided into four parts: the quasi-periodic solutions in regions I and II, the quasi-periodic solutions in region III, the complicated homoclinic orbits, and the chaotic orbits between these invariant sets. The first two parts can be analysed by KAM theory and Aubry-Mather theory, see Section 4 and the Figure 8. The perturbed invariant manifolds can be computed using the method in this paper (see Appendix B and the Figure 13) or be analysed by using the classical Menilkov method [10]. For the chaotic orbits

between these invariant sets, to the best of our knowledge, the Smale-Birkhoff theorem [27, Theorem III.17] can be used to depict such stochastic orbits.

For $\epsilon = 0.8$, it can be seen from Figure 9 that there are chaotic dynamics in the low energy region. A branch of the unstable manifold, shown in Figure 15, prevents the existence of quasi-periodic solutions in regions I and II. Moreover, the unstable manifold is trapped in the neighbourhood of $(\xi, 0)$, and the folds near $(\xi, 0)$ (Figure 16) are quite convoluted. It is anticipated that there exists tangency between the unstable manifold and the impact surface $\{(x, y, t) : x = \xi\}$.

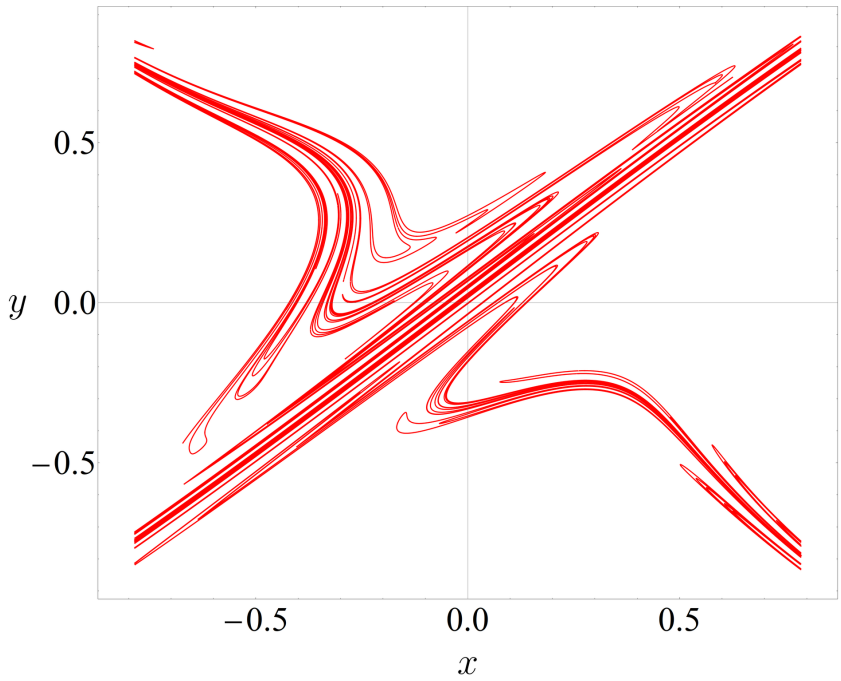

Figure 11: A branch of unstable manifold.

6. Concluding remarks

In this work, we prove the existence of invariant tori for an impact inverted pendulum both in low and high energy via KAM theory. The homoclinic bifurcation is discussed by a new numerical method, which provides tools for the computation of the discontinuous invariant manifold in impact systems. When the perturbation gets large, there exists tangency between the unstable manifold and the impact surface. In such case, the folds of the invariant manifold is very complicated in the neighbourhood of the tangent point. There are theories [6, 22] discussing about the case of tangency between the stable manifold and the unstable manifold. However, to the best of our knowledge, the case of tangency between the invariant manifold and the impact surface is still open. There is numerical evidence in this work that the invariant manifold may be trapped in the neighbourhood of the grazing point.

Appendix A: Estimate of the main remainders

In this Section, we prove the main estimates (4.6) and (4.11). We restate it in here for convenience.

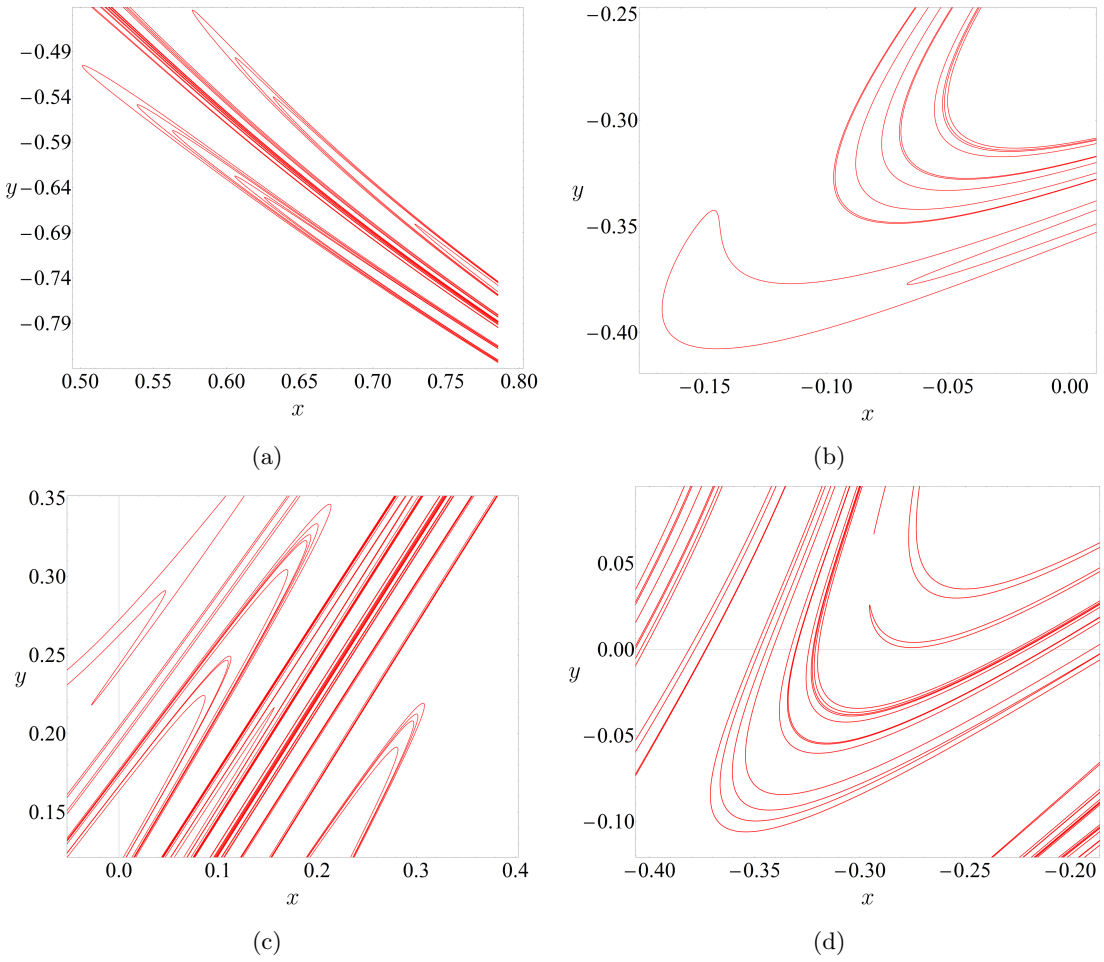

Figure 12: Magnifications of a branch of the unstable manifold.

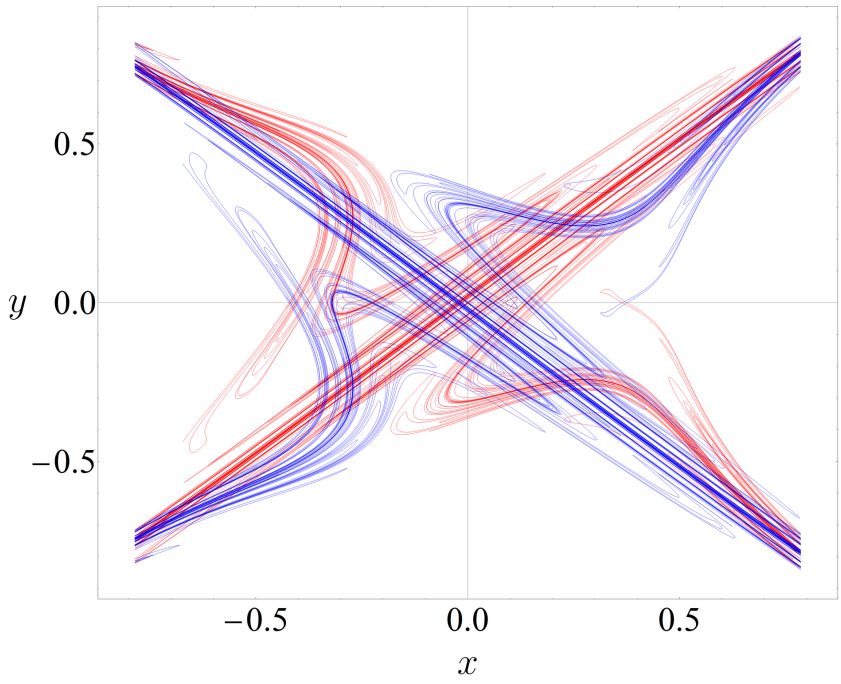

Figure 13: The stable manifold (blue) and the unstable manifold (red).

Proposition A.1. **(i)** *There exists positive constants ϵ_0, a such that for any $\epsilon \in [0, \epsilon_0]$ the following estimates*

$$|I''(H)| \geq a > 0 \text{ and } |\frac{\partial^{k+l}}{\partial H^k \partial t^l} N_i(H,t)| \leq C\epsilon$$

hold on $(H,t) \in [h_0, h_1] \times S^1$ for all $0 \leq k+l \leq 4$, $i = 1, 2$, if

$$|\frac{\partial^{k+l}}{\partial x^k \partial t^l} V| \leq \epsilon \leq \epsilon_0 \tag{A.1}$$

on $(x,t) \in [-\xi, \xi] \times S^1$ for all $0 \leq k+l \leq 5$, where C is a constant independent of ϵ.

(ii) *There exists constant $\epsilon_1 > 0$ such that for any $\epsilon \in (0, \epsilon_1)$ the following estimate*

$$\epsilon^3 |\frac{\partial^{k+l}}{\partial Q^k \partial \bar{P}^l} R_i(Q, \bar{P}, \epsilon)| \leq \epsilon^{1+\nu}$$

holds on $(\bar{P}, Q) \in [1,2] \times S^1$ for all $0 \leq k+l \leq 4$, $i = 1, 2$, where $\nu > 0$ is a constant independent of ϵ.

Lemma A.1. *With the notations in Section 3.2, $I(h)$ is C^∞ and $I'(h) > 0, I''(h) > 0$ on $h \in [h_0, h_1]$ for any interval $[h_0, h_1] \subset (\cos\xi, 1)$.*

Proof. Note that

$$I'(h) = 2\sqrt{2} \int_0^{\arccos h - \xi} \frac{dx}{\sqrt{h - \cos(x - \xi)}} = T(h),$$

where $T(h)$ is the period of closed orbit with energy h for $h \in (\cos\xi, 1)$. We first derive the expression of the period of the pendulum.

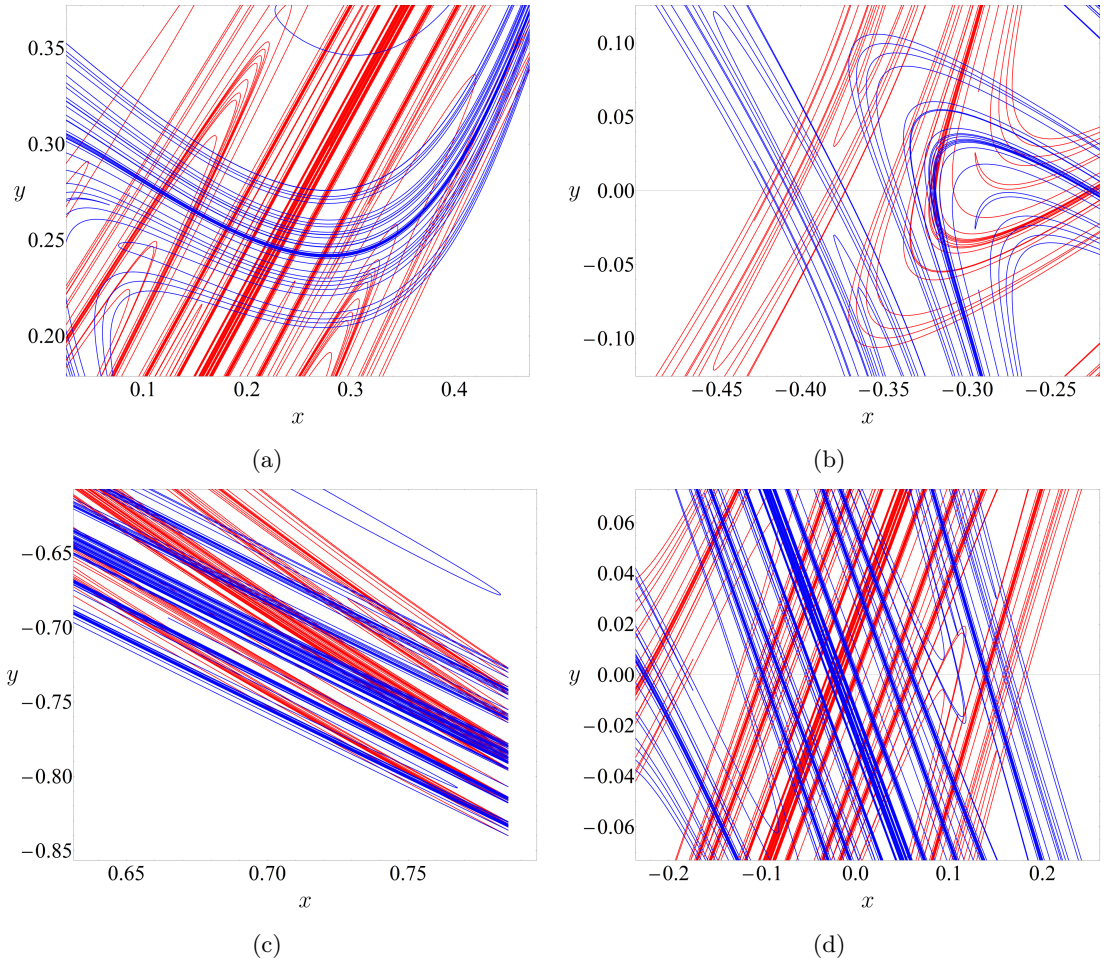

Figure 14: Magnifications of the intersections of stable and unstable manifolds.

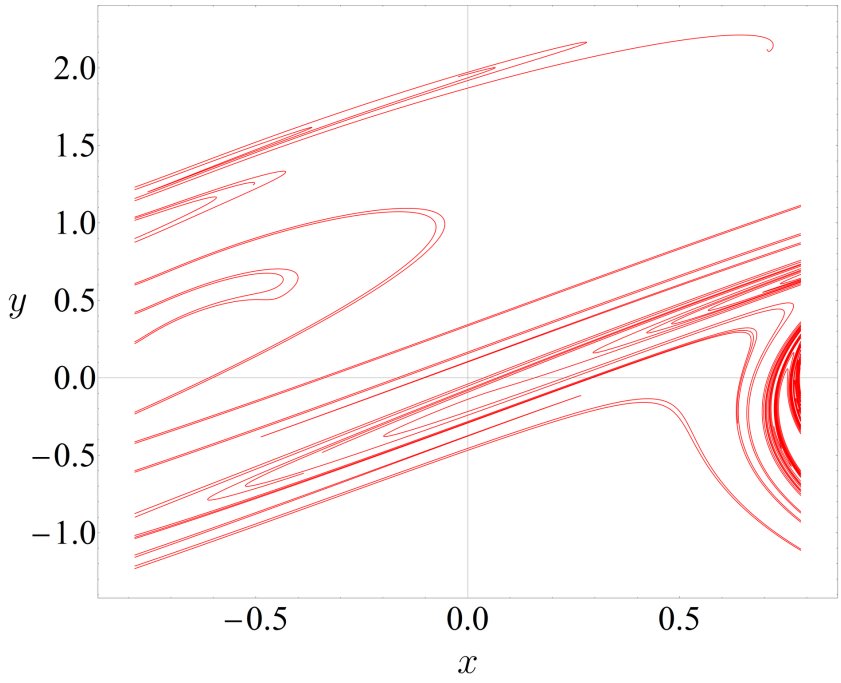

Figure 15: A branch of the unstable manifold for $\epsilon = 0.8$.

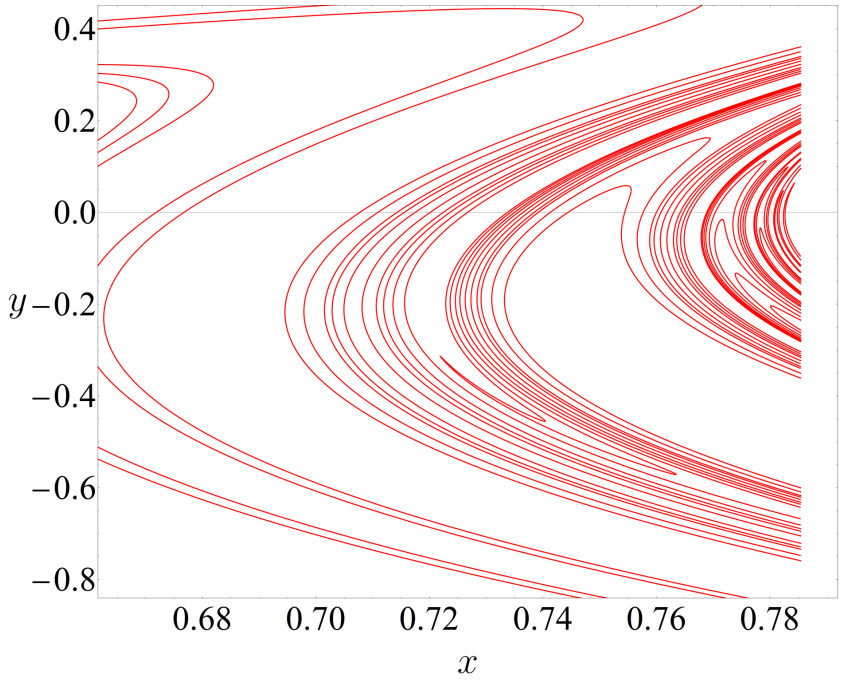

Figure 16: The Magnification of Figure 15.

Consider the Hamiltonian of classical pendulum

$$H(y,x)=\frac{1}{2}-\cos x.$$

We consider the energy level $h\in(0,1)$, i.e., the oscillatory case. Let the lagrest angle of the pendulum be θ_0, i.e., $-h=\cos\theta_0$. Set

$$\sin\frac{x}{2}=\sin\frac{\theta_0}{2}\sin\varphi. \tag{A.2}$$

If the integral interval is $x\in[0,\theta_0]$, then $\varphi\in[0,\frac{\pi}{2}]$. Hence, we have

$$\frac{dy}{dt}=-\sin x=-2\sin\frac{x}{2}\cos\frac{x}{2}=-2\sin\frac{\theta_0}{2}\sin\varphi\sqrt{1-\sin^2\frac{\theta_0}{2}\sin^2\varphi}.$$

Because of

$$\begin{aligned}y=&\sqrt{2(h+\cos x)}\\=&\sqrt{2(-\cos\theta_0+\cos x)}\\=&\sqrt{2}\sqrt{-(1-2\sin^2\frac{\theta_0}{2})+(1-2\sin^2\frac{\theta_0}{2}\sin^2\varphi)}\\=&2\sin\frac{\theta_0}{2}\cos\varphi,\end{aligned}$$

we have

$$dy=-2\sin\frac{\theta_0}{2}\sin\varphi d\varphi.$$

Hence,

$$-\frac{2\sin\frac{\theta_0}{2}\sin\varphi d\varphi}{dt}=-2\sin\frac{\theta_0}{2}\sin\varphi\sqrt{1-\sin^2\frac{\theta_0}{2}\sin^2\varphi}.$$

The period is

$$4\int_0^{\frac{\pi}{2}}\frac{d\varphi}{\sqrt{1-\sin^2\frac{\theta_0}{2}\sin^2\varphi}}, \tag{A.3}$$

where $\theta_0=\arccos -h$.

After moving the wall from $x=0$ to $x=\pi-\xi$, by (A.2) and (A.3) we have

$$\begin{aligned}I'(h)=T(h)&=2\sqrt{2}\int_0^{\arccos h-\xi}\frac{dx}{\sqrt{h-\cos(x-\xi)}}\\&=4\int_{K(h)}^{\frac{\pi}{2}}\frac{d\varphi}{\sqrt{1-\sin^2(\frac{\arccos -h}{2})\sin^2\varphi}},\end{aligned} \tag{A.4}$$

where $K(h)$ satisfies

$$\sin\frac{\pi-\xi}{2}=\sin\frac{\arccos -h}{2}\sin K(h),$$

so,

$$K(h)=\arcsin\frac{\cos\frac{\xi}{2}}{\sin\frac{\arccos -h}{2}}.$$

Since the denominator in (A.4) does not vanish for any $h \in [h_0, h_1] \subset (\cos\xi, 1)$, it is clear that $I'(h)$ is C^∞. By direct computation, we have

$$I''(h) = T'(h) = 4\int_{K(h)}^{\frac{\pi}{2}} \frac{d\varphi}{(1-\sin^2\frac{\arccos -h}{2}\sin^2\varphi)^{3/2}} - 4\frac{K'(h)}{\sqrt{1-\cos^2\frac{\xi}{2}}}, \tag{A.5}$$

where

$$K'(h) = -\frac{\cos\frac{\xi}{2}\cos\frac{\arccos -h}{2}}{2\sqrt{1-h^2}\sqrt{\sin^4\frac{\arccos -h}{2} - \sin^2\frac{\arccos -h}{2}\cos^2\frac{\xi}{2}}}.$$

It follows that $I''(h) > 0$ for $h \in (\cos\xi, 1)$ and $I''(h) \to \infty$ as $h \to 1$ or $h \to \cos\xi$. □

We call a function to be differentiable in a closed set if it is differentiable in an open set that contains the closed set. The proof of the following Lemma is followed by the Implicit Function Theorem.

Lemma A.2. *Let $y = f(x) + f_1(x, w, z)$, where $f : [x_0, x_1] \to \mathbb{R}$ such that $f'(x) \geq \delta$ on $[x_0, x_1]$, $f_1 : [x_0, x_1] \times K$ is a C^r function, where $K \subset \mathbb{R}^2$ is compact set and $r \geq 1$. Then there exists $\epsilon_0 > 0$ such that the inverse of x has the following form*

$$x = f^{-1}(y) + g_1(y, w, z),$$

and

$$|\frac{\partial^{k+l+m}}{\partial y^k \partial w^l \partial z^m} g_1| \leq c_2\epsilon$$

for all $k + l + m \leq r$ and $(y, w, z) \in [f(x_0) + O(\epsilon), f(x_1) + O(\epsilon)] \times K$ and c_2 is a constant only dependent on δ, if

$$|\frac{\partial^{k+l+m}}{\partial y^k \partial w^l \partial z^m} f_1| \leq c_1\epsilon$$

holds for for all $k + l + m \leq r$ and $(x, w, z) \in [x_0, x_1] \times K$.

Proof of Proposition A.1. : By Lemma A.1, for $H \in [h_0, h_1] \subset (\cos\xi, 1)$ we have $I''(H) \geq a > 0$. Let $I_0 = h^{-1}(h_0) = I(h_0)$ and $h_1 = h^{-1}(h_1) = I(h_1)$. We first take an interval $[I_0 - \delta, I_1 + \delta]$ such that $[h(I_0 - \delta), h(I_1 + \delta)] \subset (\cos\xi, 1)$ for $\delta > 0$. Since we only consider the motion in $\theta \in [0, \frac{1}{2}]$, i.e., $x \geq 0$, (4.3) has the form

$$H(I, \theta, t) = h(I) + V(x(I, \theta) - \xi, t).$$

Since $x(I, \theta)$ is C^r bounded on $[I_0 - \delta, I_1 + \delta] \times [0, \frac{1}{2}]$, by (A.1) we have

$$|\frac{\partial^{k+l+m}}{\partial I^k \partial\theta^l \partial t^m} V(x(I, \theta) - \xi, t)| \leq C\epsilon$$

on $(I, \theta, t) \in [I_0 - \delta, I_1 + \delta] \times [0, \frac{1}{2}] \times S^1$ for all $k + l + m \leq 5$. By Lemma A.2, we have

$$|\frac{\partial^{k+l+m}}{\partial H^k \partial t^l \partial\theta^m} I_1(H, t, \theta)| \leq C_1\epsilon$$

on $(H, t, \theta) \in [h(I_0 - \delta) + O(\epsilon), h(I_1 + \delta) + O(\epsilon)] \times S^1 \times [0, \frac{1}{2}]$ for all $k + l + m \leq 5$. Since $h(I)$ is a strictly increasing function, we can take ϵ_0 sufficiently small such that

$$[h(I_0), h(I_1)] \subset [h(I_0 - \delta) + O(\epsilon), h(I_1 + \delta) + O(\epsilon)] \subset (\cos\xi, 1)$$

for $\epsilon \in (0, \epsilon_0)$. Hence, in particular we have

$$|\frac{\partial^{k+l+m}}{\partial H^k \partial t^l \partial \theta^m} E_i(H,t,\theta)| \le C_1 \epsilon \tag{A.6}$$

on $(H,t,\theta) \in [h(I_0), h(I_1)] \times S^1 \times [0, \frac{1}{2}]$ for all $k+l+m \le 4$ and $i = 1,2$, where $E_1 = \frac{\partial I_1}{\partial H}$ and $E_2 = -\frac{\partial I_1}{\partial t}$. Since we integrate (4.4) on $\theta \in [0, \frac{1}{2}]$, N_i has the same estimate as (A.6) ([18, Lemma 1]). The proof of **(i)** is complete.

Similarly, for the proof of **(ii)**, we take an interval $[2\xi - \delta, 4\xi + \delta]$ for a constant $\delta > 0$. Note that $p \in [2\xi - \delta, 4\xi + \delta]$ implies that $|y| \in [\frac{2\xi - \delta}{\epsilon}, \frac{4\xi + \delta}{\epsilon}]$. By (4.7) and Lemma A.2, we have

$$\epsilon^2 |\frac{\partial^{k+l+m}}{\partial F^k \partial |q|^l \partial (\epsilon T)^m} G| \le c_1 \epsilon^2$$

on

$$(F, |q|, \epsilon T) \in [(2\xi - \delta)^2/2 + O(\epsilon^2), (4\xi + \delta)^2/2 + O(\epsilon^2)] \times [0, 2\xi] \times S^1$$

for all $k+l+m \le 5$. Hence, in particular we have

$$\epsilon^3 |\frac{\partial^{k+l}}{\partial P^k \partial Q^l} F_i(P, Q, |s|)| \le c_1 \epsilon^3$$

on $(P, Q, |s|) \in [(2\xi)^2/2, (4\xi)^2/2] \times S^1 \times [0, 2\xi]$ for all $k+l+m \le 4$, where $F_1 = \frac{\partial G}{\partial Q}$ and $E_2 = -\frac{\partial G}{\partial P}$. It follows that

$$\epsilon^3 |\frac{\partial^{k+l}}{\partial \bar{P}^k \partial Q^l} G_i(\bar{P}, Q, |s|)| \le c_2 \epsilon^3 \tag{A.7}$$

on $(\bar{P}, Q, |s|) \in [1,2] \times S^1 \times [0, 2\xi]$ for all $k+l+m \le 4$ and $i = 1,2$. Since we integrate (4.9) on $s \in [-2\xi, 2\xi]$, R_i has the same estimate as (A.7). Let c_3 be the constant such that

$$\epsilon^3 |\frac{\partial^{k+l}}{\partial \bar{P}^k \partial Q^l} R_i(\bar{P}_0, Q_0, \epsilon)| \le c_3 \epsilon^3.$$

Take ϵ_1 sufficiently small such that $c_3 \epsilon^3 \le \epsilon^{1+\nu}$ for some $\nu > 0$ when $\epsilon \in (0, \epsilon_1)$. This completes the proof. □

Appendix B: The numerical computation of invariant manifolds under the effect of impacts

We restate the equation in here:

$$\begin{aligned} \dot{x} &= y, \\ \dot{y} &= \sin x - V_x(x,t). \end{aligned} \tag{B.1}$$

We assume V is T-periodic with respect to t in here. When V is small, there exists an unique saddle type T-periodic solution near $(0,0)$, i.e., a fixed point of the time-T-map. First, we need to locate the saddle fixed point. This can be done by using the classical shooting method. Let the time-T-map from $t = 0$ to $t = T$ be denoted by ϕ. Suppose that the eigenvectors and the corresponding eigenvalues of $\mathrm{D}\phi(X^*)$ are $v_1, v_2, \lambda_1, \lambda_2$, where $X^* = (x^*, y^*)$ is the saddle point of ϕ. Without loss of generality, assume that $\lambda_1 > 1$ and $\lambda_2 < 1$.

We only state next how to compute the unstable manifold, and the case of the stable manifold is similar.

(1) We take a very short line segment started at X^* that has the same direction as v_1. Denote this segment by l_0. We select some points increasingly or decreasingly in l_0:

$$A_0 = \{X_1, X_2, \cdots, X_N\},$$

where $X_1 = X^*$ and X_N is some other endpoint of l_0. Then we map these points by ϕ to obtain

$$\phi(A_0) = \{\phi(X_1), \phi(X_2), \cdots, \phi(X_N)\}.$$

We choose the segment l_0 small enough so that any solution started at $X_i \in A_0$ does not have impact with $|x| = \xi$. Note that $\phi(X_1) = X_1$, then we can select the points in $\phi(A_0)$ that satisfy

$$||\phi(X_i) - X_1|| \geq ||X_N - X_1||, \tag{B.2}$$

where $||\cdot||$ is the Euclidean norm. Let

$$\bar{A}_0 = \{X_N, \phi(X_n), \phi(X_{n+1}), \cdots, \phi(X_N)\},$$

where X_i satisfies (B.2) for $n \leq i \leq N$.

(2) The continuation of $\bar{A}_0$ is via the modified parametric method, which is described as follows. We interpolate the set $\bar{A}_0$ by a parametric curve p_0 numerically such that

$$p_0(\frac{i-1}{\#(\bar{A}_0) - 1}) = \text{index}[\bar{A}_0](i), \tag{B.3}$$

where $\#$ is the cardinality of a set and index$[\cdot]$ is a map such that index$[C](i)$ is the i-th element of the finite set C. So we have $p_0 : [0,1] \to \mathbb{R}^2$ and $p_0(0) = X_N$, $p_0(1) = \phi(X_N)$. We associate each point in $\bar{A}_0$ with its parametric coordinate to obtain a new set:

$$\tilde{A}_0 = \{(X_N, 0), \cdots, (\phi(X_N), 1)\}.$$

Then we define a map $\bar{\phi}$ such that

$$\bar{\phi}((X, s)) = (\phi(X), s, n),$$

where n is the impact times of the orbit $\phi^t(X)$ during $t \in [0, T]$ ($\phi^t(X)$ is the solution initiated at X for $t = 0$). Map the set $\tilde{A}_0$ by $\bar{\phi}$. And then we partition the set $\bar{\phi}(\tilde{A}_0)$ by the change of the last coordinate. Let the sets after partition be

$$\{A_1^1, A_2^1, \cdots, A_k^1\}.$$

(3) The change of the last coordinate corresponds to the collision of unstable manifold with the impact surface. Now we present an approach to locate the intersection of the unstable manifold and the impact surface. For example, let the last element of A_1^1 and the first element of A_2^1 be (X_j, s_j, n_j) and $(X_{j+1}, s_{j+1}, n_{j+1})$. If the following inequality holds

$$||(x_j, |y_j|) - (x_{j+1}, |y_{j+1}|)|| \leq \delta_1, \tag{B.4}$$

where $X_j = (x_j, y_j)$ and $X_{j+1} = (x_{j+1}, y_{j+1})$, $0 < \delta_1 \ll 1$ is a constant, and we do not change the sets A_1^1 and A_2^1. If (B.4) does not hold, we add the element

$$\bar{\phi}((p_0(\frac{1}{2}(s_j + s_{j+1})), \frac{1}{2}(s_j + s_{j+1}))$$

to the end position of set A_1^1 or the first position of set A_2^1 if the last coordinate of this element is same as n_j or n_{j+1}. If the set A_1^1 or A_2^1 has changed, then we repeat this process until (B.4) holds. We deal with every adjoining sets A_j^1 and A_{j+1}^1 by above operation, and we can thus conclude numerical procedure.

(4) To get enough accurate parametric curves, we have to insure that the phase coordinates of any adjoining elements in A_i^1 are not too far away. More precisely, if the distance

$$||X_i - X_{i+1}|| \leq \delta_2, \tag{B.5}$$

we do not add points between (X_i, s_i, n_i) and $(X_{i+1}, s_{i+1}, n_{i+1})$, where (X_i, s_i, n_i) and $(X_{i+1}, s_{i+1}, n_{i+1})$ are a pair of adjoining elements of A_j^1. If (B.5) does not hold, we add m points

$$\bar{\phi}((p_0(s_i + d_1), s_i + d_1)), \cdots, \bar{\phi}((p_0(s_i + d_m), s_i + d_m))$$

between (X_i, s_i, n_i) and $(X_{i+1}, s_{i+1}, n_{i+1})$, where

$$d_l = \frac{l(s_{i+1} - s_i)}{m+1}$$

for $1 \leq l \leq m$. We apply this process to every adjoining elements in A_j^1 to obtain a new set which we still denote it by A_j^1. Then we repeat this whole process until A_j^1 does not change any longer, i.e., (B.5) holds for any pair of adjoining elements in A_j^1. After applying the operation to every A_l^1 for $1 \leq l \leq k$, we obtain the interpolation data for the next parametrisation.

(5) We remove the last two coordinates for every elements of A_l^1 for $1 \leq l \leq k$. Then we parametrize each A_i^1 as (B.3) by p_i^1. Now we get the data for the next continuation and its parametric curves

$$\{A_1^1, A_2^1, \cdots, A_k^1\}, \{p_1^1, p_2^1, \cdots, p_k^1\}.$$

This completes one time iteration.

We apply the procedures **(2)**-**(5)** to each pair of A_i^1 and p_i^1 to obtain the second time continuation data and its parametric curves:

$$\{A_{1,1}^2, A_{1,2}^2, \cdots, A_{1,l_1}^2, A_{2,1}^2, A_{2,2}^2, \cdots, A_{2,l_2}^2, \cdots, A_{k,1}^2, A_{k,2}^2, \cdots, A_{k,l_k}^2\},$$
$$\{p_{1,1}^2, p_{1,2}^2, \cdots, p_{1,l_1}^2, p_{2,1}^2, p_{2,2}^2, \cdots, p_{2,l_2}^2, \cdots, p_{k,1}^2, p_{k,2}^2, \cdots, p_{k,l_k}^2\},$$

where $A_{i,j}^2$ and $p_{i,j}^2$ are generated by A_i^1 and p_i^1 for $1 \leq j \leq l_i$. Hence, we can iterate this procedure to obtain the 3th,4th,$\cdots$ times parametric curves.

We can apply the same procedure to another short segment started at X^* and it has the same direction as $-v_1$. Finally, we complete the computation of unstable manifold. We can obtain the stable manifold by replacing ϕ and v_1 with ϕ^{-1} and v_2.

Remark 4. *We can also choose the initial segment as a quadratic curve instead of a straight line segment. To determine this quadratic curve we have to compute the second order variational equation of* (B.1) *in the neighbourhood of the saddle periodic solution.*

Remark 5. *The procedures* **(3)** *and* **(4)** *add many points in* A_i^1 *so that the coordinate for impact times in this set can have another value, so we have to partition* A_i^1 *again to insure that the coordinate for impact times of every element is the same in* A_i^1.

Remark 6. *For the non-conservative impact, i.e.,* $y \to -ry$ *when* $|x| = \xi$, *where* $0 < r < 1$ *is a constant, we can replace the criterion* (B.4) *by*

$$||(x_j, r|y_j|) - (x_{j+1}, |y_{j+1}|)|| \leq \delta_1$$

when we compute the unstable manifold. For the case of the stable manifold, the corresponding criterion is

$$||(x_j, |y_j|) - (x_{j+1}, r|y_{j+1}|)|| \leq \delta_1.$$

Acknowledgments

The authors are grateful to the anonymous referees for a careful reading and suggestions that led to an improvement of the paper. This work is supported by the National Natural Science Foundation of China (12172306,11732014).

[1] V. I. Arnold. On the behavior of an adiabatic invariant under a slow periodic change of the Hamiltonian. *DAN*, 142(4):758–761, 1962.

[2] V. I. Arnold. *Mathematical Methods of Classical Mechanics*. Springer, NewYork, 1978.

[3] V. Bangert. Mather sets for twist maps and geodesics on tori. *Dynamics reported*, 1:1–56, 1988.

[4] Z. B. Cao, C. Grebogi, D. H. Li and J. H. Xie. The Existence of Aubry-Mather sets for the Fermi-Ulam Model. *Qualitative Theory of Dynamical Systems*, 20:1–12, 2021.

[5] Z. B. Cao, X. M. Zhang, D. H. Li, S. Yin and J. H. Xie. Existence of invariant curves for a Fermi-type impact absorber. *Nonlinear Dynamics*, 99:2647–2656, 2020.

[6] F. J. Chen, A. Oksasoglu and Q. D. Wang. Heteroclinic tangles in time-periodic equations. *Journal of Differential Equations*, 254(3):1137-1171, 2013.

[7] S. N. Chow and S. W. Shaw. Bifurcations of subharmonics. *Journal of Differential Equations*, 65(3):304–320, 1986.

[8] R. Dieckerhoff and E. Zehnder. Boundedness of solutions via the twist-theorem. *Annali della Scuola Normale Superiore di Pisa-Classe di Scienze*, 14(1):79–95, 1987.

[9] Z. D. Du, Y. R. Li, J. Shen and W. N. Zhang. Impact oscillators with homoclinic orbit tangent to the wall. *Physica D*, 245(1):19–33, 2013.

[10] Z. D. Du and W. N. Zhang. Melnikov method for homoclinic bifurcation in nonlinear impact oscillators. *Computers and Mathematics with Applications*, 50:445–458, 2005.

[11] J. M. Gao and Z. D. Du. Homoclinic bifurcation in a quasiperiodically excited impact inverted pendulum. *Nonlinear Dynamics*, 79(2):1061–1074, 2015.

[12] A. Granados, S. J. Hogan and T. M. Seara. The Melnikov method and subharmonic orbits in a piecewise smooth system. *SIAM Journal on Applied Dynamical Systems*, 11(3):801-803, 2012.

[13] D. Hobson. An efficient method for computing invariant manifolds of planar maps. *Journal of Computational Physics*, 104(1):14–22, 1993.

[14] M. Kunze, T. Küpper, T and J. You. On the application of KAM theory to discontinuous dynamical systems. *Journal of Differential Equations*, 139(1):1–21, 1997.

[15] M. Levi. KAM theory for particles in periodic potentials. *Ergodic Theory and Dynamical Systems*, 10(4):777–785, 1990.

[16] M. Levi. Quasiperiodic motions in superquadratic time-periodic potentials. *Communications in Mathematical Physics*, 143(1):43–83, 1991.

[17] A. M. Mancho, D. Small, S. Wiggins and K. Ide. Computation of stable and unstable manifolds of hyperbolic trajectories in two-dimensional, aperiodically time-dependent vector fields. *Physica D*, 182:188–222, 2003.

[18] S. Marò. Relativistic pendulum and invariant curves. *Discrete and Continuous Dynamical Systems - Series A (DCDS-A)*, 35(3):1139–1162, 2014.

[19] J. Mawhin. Global results for the forced pendulum equation. *Handbook of Differential Equations*, 1:533–589, 2004.

[20] J. N. Mather. Existence of quasi-periodic orbits for twist homeomorphisms of the annulus. *Topology*, 21(4):457–467, 1982.

[21] J. Moser. On invariant curves of area-preserving mappings of an annulus. *Nachr. Akad. Wiss. Göttingen, II*, 1–20, 1962.

[22] S. E. Newhouse. Diffeomorphisms with infinitely many sinks. *Topology*, 13(1):9–18, 1974.

[23] R. Ortega. Asymmetric oscillators and twist mappings. *Journal of the London Mathematical Society*, 53(2):325–342, 1996.

[24] H. Rüssmann. *Über invariante Kurven differenzierbarer Abbildungen eines Kreisringes*. Nachr. Akad. Wiss. Göttingen, Math. Phys. K1. II, 67–105, 1970.

[25] S. W. Shaw and H. R. Rand. The transition to chaos in a simple mechanical system. *International Journal of Non-Linear Mechanics*, 24(1):41–56, 1989.

[26] R. L. Tian, T. Wang, Y. F. Zhou, J. Li and S. T. Zhu. Heteroclinic chaotic threshold in a nonsmooth system with jump discontinuities. *International Journal of Bifurcation and Chaos*, 2050141:1–11, 2020.

[27] E. Zehnder. *Lectures on Dynamical Systems: Hamiltonian Vector Fields and Symplectic Capacities*. European Mathematical Society, 2010.

[28] V. Zharnitsky. Invariant curve theorem for quasiperiodic twist mappings and stability of motion in the Fermi-Ulam problem. *Nonlinearity*, 13(4):1123, 2000.

[29] V. Zharnitsky. Invariant tori in Hamiltonian systems with impacts. *Communications in Mathematical Physics*, 211(2):289–302, 2000.